Available online at www.sciencedirect.com
SCIENCE DIRECT®
Journal of Power Sources 129 (2004) 312–318
JOURNAL OF POWER SOURCES
www.elsevier.com/locate/jpowsour

Highly efficient lithium composite anode with hydrophobic molten salt in seawater

Yancheng Zhang[1], Mirna Urquidi-Macdonald*,[2]

Department of Engineering Science and Mechanics, Pennsylvania State University, 0212 Earth and Engineering Science, University Park, PA 16802, USA

Received 3 October 2003; accepted 14 November 2003

Abstract

A lithium composite anode (lithium/1-butyl-3-methyl-imidazoleum hexafluorophosphate ($BMI^+PF_6^-$)/4-VLZ) for primary lithium/seawater semi-fuel-cells is proposed to reduce lithium–water parasitic reaction and, hence, increase the lithium anodic efficiency up to 100%. The lithium composite anode was activated when in contact with artificial seawater (3% NaCl solution) and the output was a stable anodic current density at 0.2 mA/cm^2, which lasted about 10 h under potentiostatic polarization at +0.5 V versus open circuit potential (OCP); the anodic efficiency was indirectly measured to be 100%. With time, a small traces of water diffused through the hydrophobic molten salt, $BMI^+PF_6^-$, reached the lithium interface and formed a double layer film (LiH/LiOH). Accordingly, the current density decreased and the anodic efficiency was estimated to be 90%. The hypothesis of small traces of water penetrating the molten salt and reaching the lithium anode—after several hours of operation—is supported by the collected experimental current density and hydrogen evolution, electrochemical impedance spectrum analysis, and non-mechanistic interface film modeling of lithium/$BMI^+PF_6^-$.

Keywords: 1-Butyl-3-methyl-imidazoleum hexafluorophosphate ($BMI^+PF_6^-$); Hydrophobic molten salt; Lithium composite anode; Lithium/seawater semi-fuel-cell

1. Introduction

A lithium/seawater battery is an attractive system as a power source for marine applications. Lithium has a negative standard electrochemical potential (−3.05 V_{SHE}) and a high unit mass electrochemical equivalence (3.86 Ah/g) [1–4]. Seawater is used as the electrolyte and does not need to be stored in the battery. However, anodic lithium–water parasitic reactions consume electrons and produce heat and hydrogen gas. Attempts to slow down or avoid lithium–water parasitic reactions and reach high anodic efficiency have been the focus of several research groups over the years [2–13]. An ion-conductive polymer membrane was used [4,5,14] to isolate the lithium metal surface from water. However, results showed that the polymer membrane swelled and lost adhesion to the lithium surface while absorbing water. In this paper, we use an hydrophobic molten salt, $BMI^+PF_6^-$, held in contact with the lithium metal by a porous membrane; the "composite" system is proposed as a substitute for the above polymer membrane. 1-Butyl-3-methylimidazole (BMI^+)-based molten salt with PF_6^- exhibits excellent chemical stability and high hydrophobicity. It possesses of an ionic conductivity of 1.8 mS/cm at 22–23 °C and a density of 1.36 g/cm^3 [15]. Its highest water absorption is estimated to be 4% [5].

The hydrophobic $BMI^+PF_6^-$ is a liquid at room temperature. The wet-ability with lithium metal was not measured but has a visually good contact. A porous membrane VLZ-105 μm (manufactured by Nippon Kodoshi Corporation, i.e. NKK) was used to hold the molten salt in contact with the lithium anode. Although the membrane absorbs water, it prevents water leakage if soaked with hydrophobic $BMI^+PF_6^-$ overnight before the assembly of the lithium composite anode. Four layers of the VLZ membrane were overlapped since the membrane was very soft and thin. A SEM image of the VLZ membrane is shown in Fig. 1.

2. Experimental

The electrochemical cell setup comprised of a lithium/$BMI^+PF_6^-$/4-VLZ composite anode as the working electrode, a nickel wire cathode, and the reference electrode (the

* Corresponding author. Tel.: +1-814-863-4217; fax: +1-814-863-7967.
E-mail address: mumesm@engr.psu.edu (M. Urquidi-Macdonald).
[1] Electrochemical Society Student Member.
[2] Electrochemical Society Active Member.

0378-7753/$ – see front matter © 2004 Elsevier B.V. All rights reserved.
doi:10.1016/j.jpowsour.2003.11.058

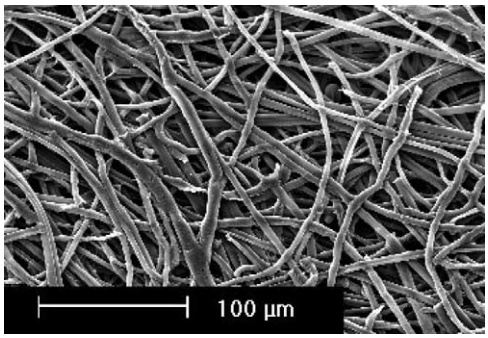

Fig. 1. SEM image of VLZ.

saturated calomel electrode, SCE), in addition to a hydrogen gas collector (a burette with an inverted funnel) as shown in Fig. 2. The nickel wire, wound in circles with the total surface area of 15 cm^2, was able to provide a large enough cathodic current so the overall cathodic reactions would not limit the output current of the lithium composite anode.

The lithium composite anode was specially designed to avoid water leakage. It was assembled in a cylindrical poly(tetrafluoroethylene) (PTFE) holder in a glove box under an argon atmosphere. The lithium surface area exposed to molten salt, as well as the membrane exposed to 3% NaCl solution, was maintained constant and equal to 0.71 cm^2. The synthesis of hydrophobic $BMI^+PF_6^-$ [5,16] is a very important process to assure the molten salt purity and high hydrophobicity.

Once the lithium composite anode was assembled in the glove box, it was installed in the cell that was submerged in artificial seawater, 3% NaCl electrolyte. All electrochemical tests, including potentiostatic polarization and electrochemical impedance spectroscopy (EIS), were measured with a Solatron SI 1280B Electrochemical Measurement System. An applied constant potential was set at +0.5 V versus OCP for the potentiostatic polarization. A small ac potential (10 mV, peak to peak) was applied for the EIS measurement and the sweep frequency ranged from 20 kHz to 0.1 Hz.

3. Results and discussion

3.1. Potentiostatic anodic polarization of lithium composite anode

After the lithium composite anode was immersed in artificial seawater, the open circuit potential (OCP) was measured to be $-2.83\,V_{SCE}$. Then potentiostatic anodic polarization was applied at $-2.33\,V_{SCE}$ (0.5 V versus OCP). The profile of the polarization current density is shown in Fig. 3. The anodic current density was stable at 0.2 mA/cm^2 for about 10 h but then decreased rapidly to 0.05 mA/cm^2 and then slowly decreased to 0.03 mA/cm^2 at the 26th hour of polarization.

After the lithium composite anode was disassembled, the lithium surface was still “shiny” and white LiOH could not be seen by the naked eye. No hydrogen gas was measurable in the gas collector at any time during the period of the polarization. The anodic efficiency was considered

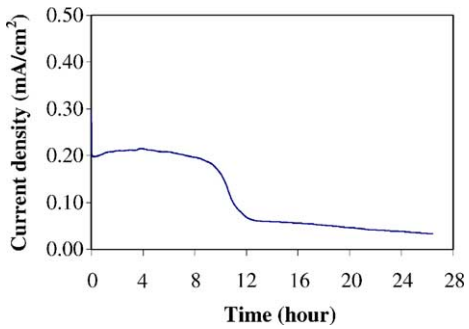

Fig. 3. Polarization current density of lithium/$BMI^+PF_6^-$/4-VLZ composite anode with polarization potential $-2.33\,V_{SCE}$ (before polarization, OCP = $-2.83\,V_{SCE}$).

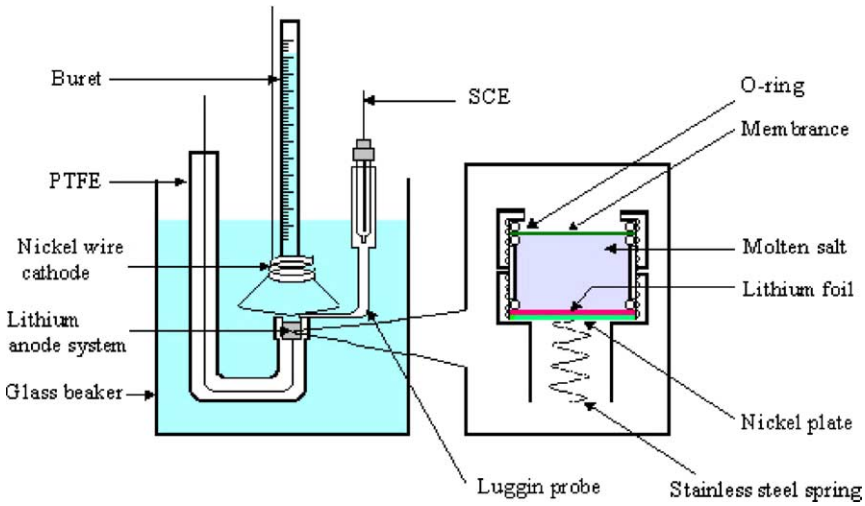

Fig. 2. Electrochemical cell setup used for electrochemical measurement of the lithium composite anode.

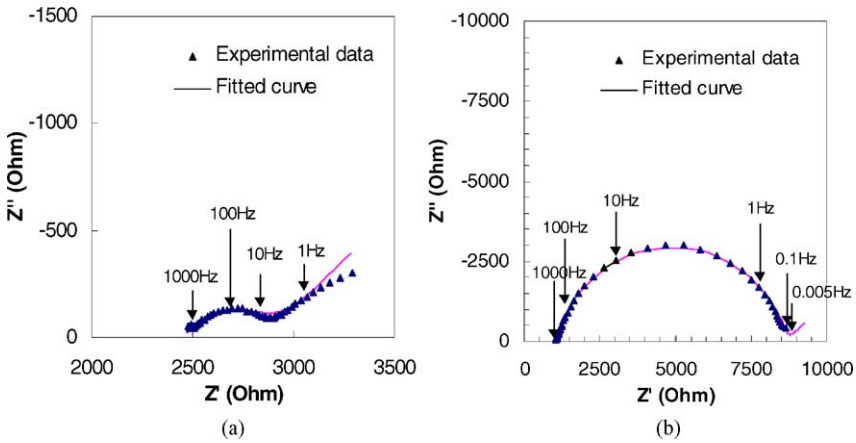

Fig. 4. Nyquist plots in complex plane for the EIS of the lithium composite anode (frequency 20 kHz to 0.1 Hz) (a) before polarization; (b) after polarization.

100% during the first 10 h of the polarization, but dropped to 90% between the 10th and 26th hour. This affect was estimated from the non-mechanistic interface film modeling of lithium/BMI$^+$PF$_6^-$ in light of the hypothesis of trace water penetration into the lithium composite anode [11,12]. This will be explained later in the paper.

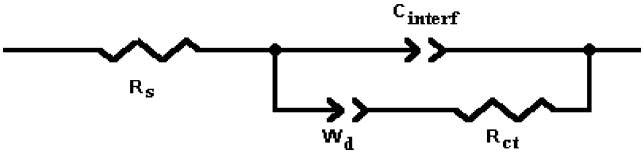

Fig. 5. An equivalent circuit model for the lithium composite anode.

3.2. Electrochemical impedance spectrum analysis

The electrochemical impedance spectra of the lithium composite anode were measured before and again after the 26-h-polarization (respectively, at $t = 0$ and 26 h as shown in Fig. 3). Before the polarization, the impedance spectrum showed two processes (Fig. 4(a)). They were a charge transfer process corresponding to the high frequency depressed capacitive loop and a mass transport process corresponding to the low frequency sloped line at about a 45° angle (in association with diffusion of electroactive species Li^+ away from the lithium surface). After the polarization, the impedance spectrum presented the disappearance of the sloped line at a frequency of larger than 0.1 Hz and the depressed capacitive loop as larger (Fig. 4(b)).

Analysis of the impedance spectra is performed using Randles equivalent circuit. From the physical characteristics of the lithium composite anode, solution resistance, R_s (including membrane resistance); diffusion impedance, W_d; charge transfer resistance, R_{ct}; and interfacial capacitance, C_{interf}; are all considered in the equivalent circuit model shown in Fig. 5. Two constant phase elements (CPEs) were used, respectively, to represent Warburg impedance, W_d; and the interfacial capacitance, C_{interf}.

A CPE's impedance is mathematically given by [17],

$$Z(\mathrm{CPE}) = Y_0^{-1}(j\omega)^{-n} \tag{1}$$

The phase angle of the constant phase element impedance is independent of the frequency and has a value of $90n^\circ$; so when $n = 1$, Z(CPE) is the impedance of a capacitor, and Y_0, capacitance. When $n = 0.5$, Z(CPE) is the Warburg impedance,

$$W_d(\mathrm{CPE}) = Y_0^{-1}(j\omega)^{-0.5} \tag{2}$$

where Y_0^{-1} represents the Warburg coefficient σ. A CPE with the exponent n of 0.5–1.0 is often used in place of a capacitor to compensate for non-homogeneity in the system. For example, a rough or porous surface can cause an interfacial capacitance to appear as a constant phase element [18–20],

$$Z(C_{interf}) = Y_0^{-1}(j\omega)^{-n} \qquad (0.5 < n < 1.0) \tag{3}$$

In Eq. (3), Y_0 can be converted into capacitance C_{interf} using the following equation [17]:

$$C_{interf} = Y_0(\omega''_m)^{n-1} \tag{4}$$

Table 1
A comparison of the component values fitted from the Nyquist plots in Fig. 4

Parameter	R_s (Ω)	R_{ct} (Ω)	$W_d = Y_0^{-1}(j\omega)^{-n}$		$Z(C_{interf}) = Y_0^{-1}(j\omega)^{-n}$			
			$\sigma = Y_0^{-1}$ (Ω)	n	Y_0 (μF s^{n-1})	n	ω''_m	$C_{interf} = Y_0(\omega''_m)^{n-1}$ (μF)
Before polarization	2453	482	640	0.5	40.6	0.58	$2\pi \times 100$	2.7
After polarization	1049	7652	62	0.5	8.0	0.83	$2\pi \times 5$	4.6

where ω''_m is the angular frequency of a maximum value in the imaginary part of the impedance (Z'').

The component values in the Randles equivalent circuit can be determined to best fit the experimental impedance spectra. The fitted curves are consistent with the experimental data in Fig. 4(a) and (b). The comparison of the component values listed in Table 1 were applied to identify the variation of the lithium/$BMI^+PF_6^-$ interface over the polarization.

The increase of charge transfer resistance, R_{ct}, from 482 to 7652 Ω explains the sharp decrease of current density during the potentiostatic polarization. Such increase of R_{ct} is indicative of the large variation of the charge transfer process which could be explained by LiH and LiOH bilayer films formed on the lithium metal surface resulting from trace water penetrating into the molten salt and reaching the lithium surface. It is assumed that the formation of the bilayer film slows down the charge transfer process compared to the process on the active lithium/$BMI^+PF_6^-$ interface. The hypothesis of trace water penetration is consistent with experiment phenomena of no noticeable (by the naked eye) white LiOH film or no measurable hydrogen evolution.

Solution resistance, R_s, (including membrane resistance) decreased from 2453 to 1049 Ω over the potentiostatic polarization, which is supposed to mainly evolve with increasing conductivity in the molten salt. Because the conductivity of seawater is high (about 60 mS/cm), the contribution from the molten salt is dominant to the R_s. Corresponding to the increase of R_s, the conductivity of the molten salt (2.5 cm thick × 0.71 cm^2) is calculated to increase from 1.44 to 3.36 mS/cm. The calculated conductivity 1.44 mS/cm before the polarization is close to the measured conductivity of BMI^+PF_6 1.2 mS/cm (a little lower than the literature value of 1.8 mS/cm). The conductivity (κ) increase has been attributed to the increase of $\sum_i (D_i \times C_i) = 5.1 \times 10^{-11}$ mol/(cm s) from the increase of ion concentrations, C_i, or diffusion coefficients, D_i, of ions in the molten salt on the assumption that the Nernst–Einstein equation is applicable to the molten salt [21,22].

$$\kappa = \sum_i \left(\frac{z_i^2 F^2 D_i C_i}{RT} \right) \tag{5}$$

where z_i is their charge number. F, R, T are, respectively, the Faraday constant, the gas constant, and the absolute temperature. Therefore, it is a reasonable postulation that the dissolution or diffusion of Li^+, Cl^-, OH^- and trace water into the molten salt increased conductivity of the molten salt resulting in the decrease of solution resistance, R_s. Furthermore, the decrease of R_s rules out the possibility of blockage of LiOH deposit in the VLZ membrane, because R_s should increase if LiOH blocks the membrane. It has shown the high initial solution resistance, R_s, before the polarization due to the low conductivity of $BMI^+PF_6^-$ was exactly the reason of the initially low current density of the polarization (0.2 mA/cm^2).

The Warburg impedance can be explained as the resultant of desorption and diffusion of the active species Li^+ away from the lithium surface controlling the lithium oxidation reaction rate at low frequency. The decrease of Warburg coefficient σ in Table 1 is presumably associated with the increase of Li^+ concentration (C_{Li^+}) and the increase of its diffusion coefficient (D_{Li^+}) through the diffusion layer, where Warburg coefficient is [21],

$$\sigma = \frac{RT}{z_i^2 F^2} \frac{1}{C_{Li^+} D_{Li^+}^{1/2}} \tag{6}$$

Trace water penetration into the molten salt tended to increase the diffusion coefficient D_{Li^+}, since D_{Li^+} is proportional to $1/\eta$ (η is viscosity coefficient in the medium) [21] and $BMI^+PF_6^-$ has a much greater dynamic viscosity (312 cP [23]) than that of water (0.890 cP [24]). The increase of Li^+ concentration in the molten salt also affected the value of the Warburg impedance that eventually decreased with experiment time. Fig. 4(b) displays a simulated low frequency sloped line (diffusion tail) close to 45° at a very low frequency (<0.005 Hz), indicating the low diffusion impedance of the active species (Li^+) away from the lithium surface.

The value of n in $Z(C_{interf})$ shows a large deviation from the value of 1 before polarization. This has been attributed to the roughness of the lithium surface [18–20] and the tortuous path of Li^+ throughout the molten salt (2.5 cm thick). After polarization, the porosity of the formed LiOH film brought a new source of the deviation of n value from 1, [18,20] while the surface roughness decreased and ionic conductivity increased in the molten salt. Note that the n values of 0.58 and 0.83 are very close to the reported data for rough and porous surfaces [20]. The value of interfacial capacitance, C_{interf}, increased from 2.7/0.71 = 3.8 to 4.6/0.71 = 6.5 μF/cm^2. If the C_{interf} after the polarization is assumed to be close to the space charge capacitance, C_{sc}, in the passive film on the lithium metal surface by neglecting the Helmholtz capacitance, the film thickness can be estimated by $C_{interf} \approx C_{sc} = \varepsilon\varepsilon_0/d$ (d is the film thickness; ε, dielectric constant; ε_0, permittivity in free space; 8.854×10^{-14} F/cm) [25,26]. If the range of ε value for the film is 10–50 (ε for LiH is 13, ε for LiOH is not available) [24,25], the film thickness, d, is obtained in the order of 20–100 Å. That is close to the reported data on the order of nanometers [11,27].

3.3. Stable lithium/$BMI^+PF_6^-$ interface

When lithium was covered with $BMI^+PF_6^-$ for 12 h in a glove box, the lithium surface remained "silvery" to the naked eye, same as a fresh lithium surface, which appears to indicate that the molten salt does not react with the lithium metal. A SEM image of this "silvery" lithium surface (after removing any liquid $BMI^+PF_6^-$ in a vacuum) is shown in Fig. 6(a). Comparably, a SEM image of a platinum surface covered by $BMI^+PF_6^-$ (after removing any

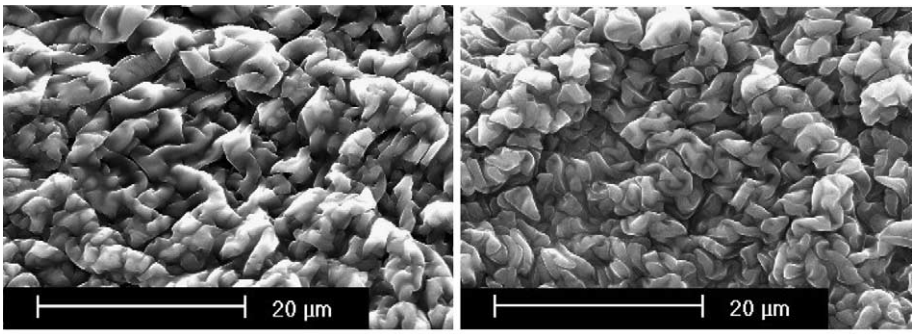

Fig. 6. (a) SEM image of a "silvery" lithium surface covered by $BMI^+PF_6^-$ (after being removed any liquid in a vacuum); (b) SEM image of a platinum surface covered by $BMI^+PF_6^-$ (after being removed any liquid in a vacuum).

liquid $BMI^+PF_6^-$ in a vacuum) is shown in Fig. 6(b). Since platinum is noble, it is assumed that the $BMI^+PF_6^-$ does not have any reaction with the platinum plate. Accordingly, the image in Fig. 6(b) represents the $BMI^+PF_6^-$ itself. The lithium surface covered with $BMI^+PF_6^-$ has a similar structure to that of the $BMI^+PF_6^-$ itself, but the former patterns look more separated, probably because of the formation of trace LiOH resulting from trace water contamination (from air when moved out of the glove box to SEM). The image similarity shows that $BMI^+PF_6^-$ did not react with the lithium surface and the surface remained "silvery". Due to the apparent non-reactivity of $BMI^+PF_6^-$ with lithium, the lithium composite anode could output stable current density for about 10 h, and could hold until lithium consumption, if nothing contaminated the stable lithium/$BMI^+PF_6^-$ interface over the time of operation.

3.4. Non-mechanistic interface film modeling of lithium/$BMI^+PF_6^-$ in artificial seawater

The interface film modeling of lithium/BMI^+PF_6 in the presence of water is shown schematically in Fig. 7 [11,13]. Three cases of different presences of water (no water, trace water, and much water) in contact with lithium/$BMI^+PF_6^-$ interface are discussed to explain the variation of the polarization current density and the maintenance of high anodic efficiency under the potentiostatic discharge of the lithium composite anode.

When no water contaminates lithium/$BMI^+PF_6^-$ interface, the interface is stable and the lithium surface maintains activity. The lithium oxidation reaction directly produces Li^+ ions, which are transported through the molten salt and 4-VLZ membranes to the seawater. Such a process is illustrated by the three interface reactions in Case 1 of Fig. 7. Reaction (I) forms Li_{Li} interstitial; reaction (II) produces Li^+ ion from the interstitial. Reactions (I) and (II) are lattice-conservative processes; neither reaction results in the formation of any film. So the sum of these two reactions, eliminating the interstitial Li_{Li}, is

$$Li \rightarrow Li^+ + V_{Li} + e^- \quad (7)$$

This reaction corresponds to the lithium oxidation reaction without forming any film on the lithium surface, which well explains how the polarization current density of the lithium composite anode kept stable for about 10 h during the first period of polarization.

Water penetration through the molten salt and onto the lithium surface is assumed to be very slow due to the high

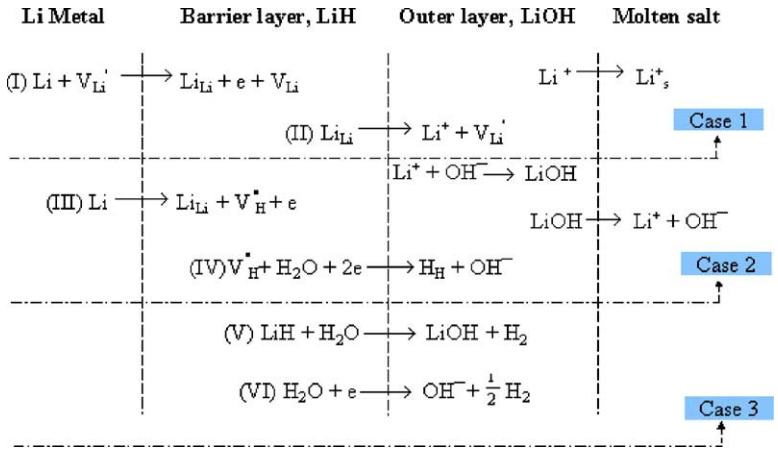

Fig. 7. Schematic diagram of interfacial reactions that occur at the interface of lithium/$BMI^+PF_6^-$.

hydrophobicity of $BMI^+PF_6^-$. But once trace water reaches the lithium/$BMI^+PF_6^-$ interface, reactions (III) and (IV) in Case 2 of Fig. 7 are activated in addition to reactions (I) and (II). Reaction (III) is lattice-non-conservative, producing Li_{Li} interstitial and $V_H^\bullet$ vacancies. The trace water is reduced and produces H_H interstitial, shown as reaction (IV). The addition of these two reactions describes the formation and growth of a defective inner layer LiH adjacent to the metal [12,13]

$$Li + H_2O + e^- \rightarrow Li_{Li} + H_H + OH^- \rightarrow LiH + OH^- \quad (8)$$

Simultaneously, the OH^- from reaction (IV) may directly combine with the Li^+ from reaction (II) and produce LiOH as the outer porous layer.

The blockage of the lithium surface by the formed LiOH layer reduces the area available for reactions (III) and (IV). The formed bilayer film, when water trace reacts at the lithium interface, is estimated to be very thin. Therefore, the lithium surface appeared to be "silvery" at the naked eye. The LiOH film and the really slow water penetration could not activate reactions (V) and (VI), and accordingly, no hydrogen gas was produced. The rapid formation of the bilayer film significantly slows down the kinetics of lithium dissolution reaction. Reaction (IV) consumes electrons and decreases the net current. Such facts can explain the quick decrease of current density in Fig. 3. This mechanism can explain the experimental phenomena that hydrogen gas was still not measurable after the sharp drop of the polarization current density.

Because reaction (IV) consumes electrons ejected from reaction (I) and reaction (III), the anodic efficiency is dropped below 100%. It was impossible to experimentally measure the consumption rate of electrons associated with reaction (IV), but the efficiency loss can be estimated to be $i_c/i_a = 10.4\%$, [11,12], if i_a represents the total rate of electron production from reaction (I) and reaction (III), and i_c represents the rate of electron consumption for reaction (IV). So the anodic efficiency $\eta(= 1 - i_c/i_a)$ is 89.6% for this case.

If larger amounts of water penetrate the lithium anode system and reach the lithium/$BMI^+PF_6^-$ interface, reactions (V) and (VI) in Fig. 7 will be activated in addition to reaction (I) to (IV). Hydrogen gas is evolved and a thick LiOH layer is formed. This scenario happened when the lithium composite anode had cell leakage, or when lithium metal was directly immersed in the seawater [11,13].

4. Conclusions

A lithium composite anode (lithium/$BMI^+PF_6^-$/4-VLZ) for primary lithium/seawater semi-fuel-cells gave a stable anodic current density at 0.2 mA/cm^2 for about 10 h under potentiostatic polarization at an overpotential +0.5 V in artificial seawater. $BMI^+PF_6^-$ does not react with lithium surfaces. Lithium oxidation reaction in the lithium composite anode produced electrons without forming any film on the lithium metal surface, and, hence, the stable lithium oxidation reaction generated a stable current density with 100% anodic efficiency. If the lithium composite anode could keep such "ideal" discharge state until lithium consumption, an applicable lithium/seawater battery will be realized.

However, the current density quickly decreased after about 10-h-polarization, and then decreased slowly. Nevertheless, the anodic efficiency η is estimated to be 90%. Trace water penetration onto the lithium surface yielded the formation of a bilayer film (LiH and LiOH) that significantly slowed down the lithium oxidation reaction originally occurring on the active lithium/$BMI^+PF_6^-$ interface. The hypothesis of trace water penetration into the lithium composite anode is consistent with the experimental phenomena of no noticeable white LiOH film or no observable H_2 and more importantly, the high hydrophobicity of $BMI^+PF_6^-$. Furthermore, trace water penetration has been demonstrated to be in agreement with the electrochemical impedance spectrum analysis and non-mechanistic interface film modeling of lithium/$BMI^+PF_6^-$.

Acknowledgements

The authors gratefully acknowledge the financial support of this work by Dr. Richard T. Carlin and Office of Naval Research (Arlington, VA) under Grant no. N00014-99-1-0446.

References

[1] D. Linden, Handbook of Batteries, second ed., McGraw-Hill, 1994.
[2] N. Shuster, Lithium–water power source for low power long duration undersea application, in: Proceedings of the 35th International Power Sources Symposium, IEEE, 1992, p. 118.
[3] N. Shuster, US Patent, #5,427,873, June 27, 1995.
[4] J.R. Flores, Electrochemical Studies of Lithium/Water Systems for the Development of Long Life-Low Power Aqueous Lithium Battery, Master thesis, Pennsylvania State University, 1999.
[5] J.J. Cho, M. Urquidi-Macdonald, Technical Report to the Office of Naval Research (Arlington, VA): Study of Lithium Polymer-Molten Salts to Enhance Efficiency and Safety in Lithium–Water Batteries, 2000.
[6] E.L. Littauer, K.C. Tsai, J. Electrochem. Soc. 123 (6) (1976) 771.
[7] E.L. Littauer, W.R. Momyer, K.C. Tsai, J. Power Sources 2 (1977) 163.
[8] E.L. Littauer, K.C. Tsai, J. Electrochem. Soc. 124 (1977) 850.
[9] E.L. Littauer, K.C. Tsai, R.P. Hollandsworth, J. Electrochem. Soc. 125 (1978) 845.
[10] O. Pensado-Rodríguez, J.R. Flores, M. Urquidi-Macdonald, D.D. Macdonald, J. Electrochem. Soc. 146 (4) (1999) 1302.
[11] O. Pensado-Rodríguez, J.R. Flores, M. Urquidi-Macdonald, D.D. Macdonald, J. Electrochem. Soc. 146 (4) (1999) 1326.
[12] O. Pensado-Rodríguez, The Electrochemistry of Lithium in Alkaline Solutions: a Model for the Film on the Metal Surface, Ph.D. thesis, Pennsylvania State University, 1998.
[13] M. Urquidi-Macdonald, D.D. Macdonald, O. Pensado-Rodríguez, J.R. Flores, Electrochim. Acta 47 (2001) 833.
[14] M. Urquidi-Macdonald, J.J. Cho, Study of lithium polymer interface to enhance efficiency and safety in lithium/water batteries, in: Proceedings of IMECE: 2000 International Mechanical Engineering

Congress and Exposition, Paper 2633 ASTM, November 5–10, Walt Disney World Dolphin, Orlando, FL.
[15] J. Fuller, A.C. Breda, R.T. Carlin, J. Electroanal. Chem. 459 (1998) 29.
[16] P. Bonhote, A.-P. Dias, N. Papageorgiou, Inorg. Chem. 35 (1996) 1168.
[17] C.H. Hsu, F. Mansfeld, Corrosion 57 (9) (2001) 747.
[18] M.W. Kendig, E.M. Meyer, G. Lindberg, F. Mansfeld, Corrosion Sci. 23 (1983) 1007.
[19] R.D. Armstrong, R.A. Burnham, J. Electroanal. Chem. 72 (3) (1976) 257.
[20] R. Delevie, Electrochemical response of porous and rough surfaces, in: P. Delahay (Ed.), Advances in Electrochemistry and Electrochemical Engineering, vol. 6, 1967, p. 329.
[21] J. Koryta, J. Dvorak, Principles of Electrochmistry, Wiley, 1987.
[22] A. Noda, M. Watanabe, in: P.C. Trulove, H.C. De Long, G.R. Stafford, S. Deke (Eds.), in: Proceedings of the 12th International Symposium on Molten Salts, vols. 99-41, The Electrochemical Society, Pennington, NJ, 1999, p. 202.
[23] R. Hagiwara, Y. Ito, J. Fluorine Chem. 105 (2000) 221.
[24] D.R. Lide, CRC Handbook of Chemistry and Physica, CRC Press LLC, 1998.
[25] J.R. Scully, D.C. Silverman, M.W. Kendig, Electrochemical Impedance: Analysis and Interpretation, ASTM, Philadelphia, PA, 1993.
[26] E. Sikora, D.D. Macdonald, J. Electrochem. Soc. 147 (2000) 4087.
[27] D.D. Macdonald, J. Electrochem. Soc. 139 (1992) 3435.